Astronomy & Astrophysics manuscript no. Fe021 February 2, 2008
(DOI: will be inserted by hand later)

Faint Hard X-ray Sources in the Galactic Center Region: Supernova Ejecta Fragments Population

A. M. Bykov

A.F. Ioffe Institute for Physics and Technology, St. Petersburg, 194021, Russia

Received

Abstract. Long *Chandra* observations of $17' \times 17'$ field in the Galactic Center (GC) region reported by Muno et al. . (2003) have revealed a population of about 2,000 hard faint X-ray sources limited by luminosities $L_{\rm x} \geq 10^{31}$ erg s^{-1}. We show that fast moving knots (FMKs) of supernovae ejecta could comprise a sizeable fraction of the sources. Each supernova event can produce hundreds of FMKs. The presence of ~ 3 supernova remnants of age $\sim 10^3$ years in the GC region could provide the required number of the FMKs. Simulated X-ray spectra of the FMKs contain both thermal and nonthermal components. The nonthermal spectra are power-laws with hard photon indexes $0 \leq \Gamma \leq 1.5$ and prominent lines of some metals (e.g. Fe). The logN–logS distribution and the hardness ratios of the FMKs in the GC region are consistent with the *Chandra* findings. Spatial distribution of the FMKs in the GC region should appear as an ensemble of coherent shell and jet-like structures of a few *arcmin*-scale.

Key words. Acceleration of particles; Radiation mechanisms: non-thermal; ISM: clouds; ISM: individual object: Galactic Center; ISM: supernova remnants; X-rays: diffuse background

1. Introduction

The unique activity of the GC appears in a number of spectacular phenomena observed in the multi-wavelength studies of the region. Apart from the enigmatic central compact source Sgr A*, there are early-type stars with more than two dozens of blue supergiants, providing the luminosity of the central parsec of $\sim 10^8\, L_\odot$, supernova remnants (SNRs), dense molecular clouds, extended magnetic structures, evidences for high star-forming activity in the past (a few 10^7 years ago) (e.g. Blitz et al. 1993; Mezger, Duschl & Zylka 1996).

X-ray observations of the GC region with sensitive high-resolution telescopes *Chandra* and *XMM − Newton* are a powerful tool to study the rich but highly obscured GC region. *Chandra* observations were performed for the Sgr A East (Maeda et al. 2002) and the GC regions (Wang, Gotthelf & Lang 2002; Baganoff et al 2003; Muno et al. 2003).

With a deep 590 ks *Chandra* exposure of a $17' \times 17'$ field in the GC region Muno et al. (2003) (M03 hereafter) catalogued 2357 X-ray sources limited by the luminosity $L_{\rm x} \geq 10^{31}$ erg s^{-1} (2.0–8.0 keV). The logN–logS distribution of the GC sources is steep around the sample limiting luminosity, indicating that the weak point sources could contribute substantially to the observed X-ray diffuse emission. The problem of the origin of the observed large scale X-ray emission from the Galactic ridge requires a careful study of possible classes of abundant hard X-ray sources with $L_{\rm x} \gtrsim 10^{29}$ erg s^{-1} (e.g. Tanaka, Miyaji & Hasinger 1999). Because of the hard spectra of the detected sources M03 suggested that accreting magnetic white dwarfs (or magnetic cataclysmic variables) and wind accreting neutron stars could be possible candidates for the sample. Moreover, Muno et al. (2003a) found periodic variability for eight sources in a sample of 285 sources and suggested that more sources in the sample could be magnetic white dwarfs or accreting pulsars. It is not yet clear, however, how many sources of the both classes are present in the GC region (M03). We shall consider here another potentially abundant class of hard X-ray sources related to supernova activity in the dense GC medium.

Multiwavelength studies of SNRs have revealed a complex structure of metal ejecta with the presence of fast moving isolated fragments of SN ejecta, interacting with the surrounding media. In the optical the multiple fast moving knots (FMKs) were observed outside the main shell of Cas A (e.g. Chevalier & Kirshner 1979; Fesen et al. 2002) and in some other SNRs. Optical FMKs in Cas A are very abundant in O-burning and Si-group elements. They have a broad velocity distribution around 6,000 km s^{-1} and apparent sizes below 0.01 pc. The optical knots in Cas A should have $L_{\rm x} \leq 10^{29}$ erg s^{-1} because of low ambient density. The similar FMKs in the dense environment of the

Send offprint requests to: e-mail: byk@astro.ioffe.ru

GC region would have $L_{\rm x} \geq 10^{30}$ erg s^{-1} with bright IR counterparts (Bykov 2002). In a low density medium only relatively big FMKs can be observed in X-rays, like the Vela shrapnel A. *Chandra* and *XMM-Newton* observations revealed there a head-tail structure with a prominent Si line, indicating that the object is a fast ejecta fragment of the scale ~ 0.3 pc (e.g. Aschenbach (2002)). Some of the hard X-ray sources detected with *XMM-Newton* in IC 443 are likely to be fragments of the SN ejecta of size below 0.1 pc interacting with a molecular cloud border (Bocchino & Bykov 2003).

In the present paper we show that an ensemble of hard X-ray sources associated with fast moving supernova ejecta fragments could be abundant and can account for some of the observed properties of the detected GC sources such as the hardness ratios and the logN–logS distribution. We simulate X-ray spectra of the FMKs of different velocities in the GC environment. In our model the hard X-ray emission of FMKs is due to both hot thermal postshock plasma and nonthermal particles accelerated at the bow shock.

2. X-ray emission of FMKs in the Galactic Center region

Consider an FMK propagating through the intercloud gas which pervades the central 50 pc. Mezger et al. (1996) estimated the gas average density of some 10^2 cm^{-3} and the mass of atomic hydrogen $\sim 10^6 M_\odot$, i.e. about one half of the total mass in this region. The matter is highly clumped. Magnetic field in the GC region is of mG strength, and provides a substantial contribution to the total pressure.

The lifetime of an FMK in a dense media is an important factor for our model and should be considered first. A fast moving knot is decelerating due to the interaction with the ambient gas. The drag deceleration time of a knot of velocity v, mass $\mathcal{M}$ and radius $\mathcal{R}$ can be estimated as $\tau_{\rm d} \sim \mathcal{M}/(\rho_{\rm a} v \pi \mathcal{R}^2) \approx 10^3 \cdot \mathcal{M}_{-3}/(n_{\rm a2}\, v_8\, \mathcal{R}^2_{-2}\,)$ years. Here $\mathcal{M}_{-3} = \mathcal{M}/10^{-3}\, M_\odot$ and $\mathcal{R}_{-2} = \mathcal{R}/(0.01{\rm pc})$. The number density $n_{\rm a2}$ of the ambient matter is measured in 100 cm^{-3} and the FMK velocity v_8 is measured in 1,000 km s^{-1}. In the inner $20'$ of the GC region the average number density $n_{\rm a} \gtrsim 100$ cm^{-3} (e.g. Mezger et al. 1996) and the fragment deceleration time $\tau_{\rm d} \lesssim 10^3$years.

The high pressure gas in the head of the fast moving ejecta fragment could drive an internal shock resulting in the knot crush and fragmentation. The internal shock velocity $v_{\rm is} \approx v/\chi^{1/2}$, where the density contrast $\chi = \rho_{\rm k}/\rho_{\rm a}$, and $\rho_{\rm a}$ and $\rho_{\rm k}$ are the ambient gas and the dense fragment densities, respectively. The knot crushing time scale $\tau_{\rm c} = \mathcal{R}/v_{\rm is}$. There are 2D hydrodynamical simulations showing that the fast knot fragmentation occurs on the timescale of $\sim (3-4)\tau_{\rm c}$ (e.g. Klein et al. 1994; Wang & Chevalier 2002). Wang & Chevalier (2002) studied the effect of density profile for core-collapsed SNe to produce the protrusions in the outer shock as observed in the Vela SNR. For the FMKs of mass $\mathcal{M}_{-3} \sim 1$ and $\mathcal{R}_{-2} \sim 1$ the fragmentation time scale is a factor of ~ 2.5 less than the drag deceleration time. However, the FMK will be a source of hard X-ray emission even at the fragmented stage if the strong forward shock is still driven by the FMK.

The hydrodynamical estimation of the inner shock velocity $v_{\rm is}$ given above assumes an efficient conversion of the bow shock ram pressure to the knot internal shock. The effects of nonthermal particle acceleration reduce the postshock gas pressure and the internal shock velocity thus increasing $\tau_{\rm c}$ (Bykov 2002). In that case the life time would be close to $\tau_{\rm d}$, unless the ablation processes. The effect of magnetic fields and nonthermal particles on the knot ablation is not yet studied.

Massive star winds would change the circumstellar environment, creating caverns of low density matter. The lifetime of fast fragments of a SN in the low density cavern should be longer than $R_{\rm b}/v_{\rm k}$, where $R_{\rm b}$ is a wind bubble size. Following the approach by Chevalier (1999) and accounting for the high pressure of the GC ambient matter one may estimate the typical scale $R_{\rm b} \sim 3$ pc, for WR, while $R_{\rm b}$ is ~ 1 pc for O9-B0 progenitor stars. The lifetimes of FMKs are $\sim 10^3$ years. The collective effect of powerful stellar winds in compact associations could blow out more extended caverns, providing somewhat longer lifetimes for the fragments of the SNe exploded inside the cavern.

Supersonic motion of the FMKs in the ambient medium result in a bow-shock/knot-shock structure heating postshock plasma and accelerating fast particles. Both thermal and nonthermal emission of postshock plasma can produce X-ray photons.

2.1. The thermal emission of FMKs

Thermal emission of hot postshock plasma could be observed from some FMKs even from the highly obscured GC region. The postshock ion temperature (measured in 10^7 K) can be estimated as $T_{\rm i7} \approx 1.4\, v_8^2$ for the simplest single-fluid case of a plasma of the solar abundance. The electron temperature just behind the strong shock is typically much lower. In the postshock layer the electron and ion temperatures equilibrate due to Coulomb collisions. The complete e-i Coulomb equilibration requires the time $t_{\rm ei} \gtrsim 3.2{\cdot}10^{11}\, T_{\rm i7}^{3/2}/n\ (s)$, where the postshock density n is in cm^{-3} (e.g. Mewe 1990). The maximal electron temperature in the postshock region can be estimated from the relation $\tau_{\rm d} \geq t_{\rm ei}$ providing $T_{\rm e7}^{\rm max} \leq 7 \cdot \mathcal{M}_{-3}^{1/2} \cdot \mathcal{R}_{-2}^{-1}$. Note that the maximal electron temperature can be achieved only for FMKs with $v_8 \geq 2.3 \cdot \mathcal{M}_{-3}^{1/4} \cdot \mathcal{R}_{-2}^{-1/2}$.

Thermal bremsstrahlung luminosity of the thin postshock plasma $\rm L_{Tx}$ is $\sim 6 \times 10^{31} \cdot \mathcal{R}^3_{-2} \cdot n^2_{\rm a2} \cdot T_{\rm e8}^{1/2}$(erg s^{-1}) (e.g. Rybicki & Lightman 1979). The effective average density in the emitting region is about 3 times that of the ambient (c.f. Wang & Chevalier (2002)). The luminosity is consistent with that observed from the GC sources in the *Chandra* catalogue of M03. However, M03 found that spectral modeling of the sources requires extremely hot

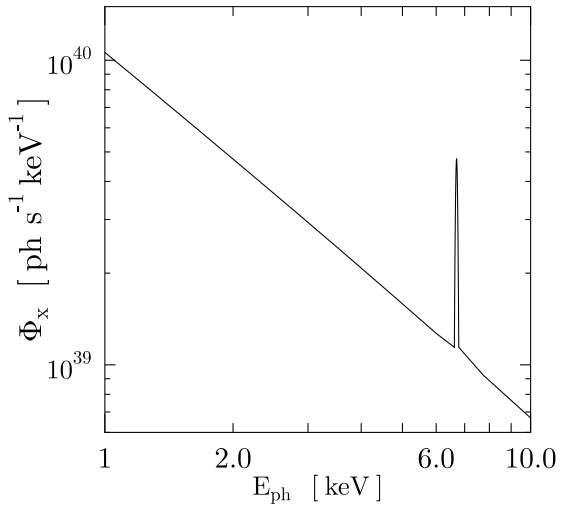

Fig. 1. Simulated nonthermal emission spectrum of an FMK of mass $\mathcal{M}_{-3} \approx 1$, radius $\mathcal{R}_{-2} = 1$ and velocity $v \approx 5,000$ km s^{-1} in an ambient medium of n = 100 cm^{-3}.

temperatures > 25 keV. That high temperatures can be expected for relatively small FMKs of $\mathcal{R}_{-2} \leq 0.3$, propagating through a dense ambient gas of $n_a \gtrsim 10^3$ cm^{-3}. In this case the deceleration time of the FMKs would be about a few hundred years.

2.2. The nonthermal emission of FMKs

Energetic nonthermal particles accelerated by Fermi mechanism in the MHD collisionless shocks diffuse through the hot postshock layer and the cold metallic knot, suffering from Coulomb losses and producing hard X-ray emission both in lines and continuum. The model of nonthermal emission of FMKs is described in details in Bykov (2002). The accelerated electron distribution was simulated using the kinetic description of charged particles interacting with a strong MHD shock. The X-ray emission is most prominent for the FMKs in dense ambient media. Energetic particle acceleration effect is expected to be efficient for strong collisionless shocks in a magnetized plasma. A significant fraction of the ram pressure could be transferred into the high energy particles. If that is the case, the postshock gas pressure drops down, affecting the reverse shock dynamics and the knot crushing conditions.

The X-ray line emission is due to K-shell ionization by nonthermal particles accelerated by the bow shock and then propagating through a metal-rich clump. Compact dense knots could be opaque for some X-ray lines. The optical depth effect due to resonant line scattering is important and is accounted for in our model.

In Fig. 1 we present a simulated spectrum of the nonthermal X-ray emission from an FMK of 0.01 pc size and mass $\mathcal{M} \approx 10^{-3}\ M_\odot$ dominated by oxygen and containing $\sim 10^{-4}\ M_\odot$ of Fe. The knot of velocity $v = 5,000$ km s^{-1} is moving through an ambient gas of $n_a = 10^2$ cm^{-3}.

The nonthermal bremsstrahlung spectrum in Fig. 1 is a power law of photon index $\Gamma \approx 1.2$ with a prominent Fe line of the equivalent width ≈ 568 eV. The spectra with $\Gamma \sim 1.2$–1.4 are typical in our simulations. The photon index is in the range $0 \leq \Gamma \leq 1.5$ and depends on the particle diffusion model inside the FMK and the rate of nonthermal ions injection (see Bykov 2002).

We simulated the dependence of the nonthermal X-ray luminosity on the fragment velocity for the same model. The power-law scaling $L_X \propto v^\zeta$ with $\zeta \approx 0.6$ fits the simulated data for the FMK velocity range $1.8 < v_8 < 7$.

We also calculated hardness ratios $hr = (h-s)/(h+s)$ for simulated spectra. The numbers of counts in the high energy band h (4.7–8.0 keV) and low band s (3.3–4.7 keV) were chosen for hard color, and h (3.3–4.7 keV) and s (2.0–3.3 keV) for medium color as in M03. For unabsorbed continuum spectra with the Fe lines simulated with an account of internal absorbtion we obtained hard color ratios $hr \sim 0.3$–0.4. Without the Fe lines the hard color ratio $hr \lesssim 0.2$. The medium color ratio was ~ 0.4.

3. The logN–logS distributions

The X-ray luminosity of an FMK depends on the fragment velocity, mass, radius, and the ambient matter. To simulate the logN–logS distribution in the homogeneous ambient medium we should know the FMK velocity and size distributions. An exact modeling of the distributions would require simulations of deceleration, expansion and ablation of an FMK as a supersonic, radiative plasmoid in a strong magnetic field (c.f. Cid-Fernandes et al. 1996). We consider here a simplified analytic model for logN–logS distributions.

3.1. The velocity distribution of FMKs

Consider SN events (of a rate $\nu_{\rm SN}(\boldsymbol{r}, t)$) ejecting $\mathcal{N}_\star$ fragments per event. The SN rate is a highly intermittent function with local variations of orders of magnitude in rich star-forming regions. The differential distribution function of the FMKs velocities and radii $\mathcal{N}(\boldsymbol{r}, \boldsymbol{v}, \mathcal{R}, t)$ satisfies

$$\frac{\partial \mathcal{N}}{\partial t} + \dot{\boldsymbol{r}}\,\frac{\partial \mathcal{N}}{\partial \boldsymbol{r}} + \dot{\boldsymbol{v}}\,\frac{\partial \mathcal{N}}{\partial \boldsymbol{v}} + \dot{\mathcal{R}}\,\frac{\partial \mathcal{N}}{\partial \mathcal{R}} = q(\boldsymbol{r}, \boldsymbol{v}, \mathcal{R}, t), \qquad (1)$$

where the source function $q(\boldsymbol{r}, \boldsymbol{v}, \mathcal{R}, t) = \nu_{\rm SN}\,\mathcal{N}_\star\,\psi(v, \mathcal{R})$. Here $\psi(v, \mathcal{R})$ is the probability distribution of the initial sizes and velocities for the FMKs. For a ballistically moving FMK the drag deceleration in the ambient medium is $\dot{\boldsymbol{v}} \propto -\rho_a v\,\boldsymbol{v}\,\mathcal{R}^2$ (for a stretched knot $\mathcal{R}$ is the transverse radius). The 2D simulations by Klein et al. (1994) and Wang & Chevalier (2002) show that the knot expansion dominate at the early evolution stages, but stops at $t > 3\tau_{\rm c}$. We can neglect the drag force at the early knot

expansion stage, while the transverse expansion is not important ($\dot{\mathcal{R}} = 0$) at the later stages where the most efficient drag deceleration of the expanded FMKs occurs.

We apply the Eq.(1) to the GC region assuming a constant rate $\nu_{\rm SN}$. The averaged distribution for $t > 3\tau_{\rm c}$ is

$$\mathcal{N}(v,\mathcal{R}) = \int_v^\infty \frac{\bar{q}(v,\mathcal{R})}{\dot{v}}\, dv, \qquad (2)$$

where $\bar{q}(v,\mathcal{R}) \propto a^{-1} q(v,\mathcal{R}/a)$ and $a(\chi)$ is an expansion factor. The transverse expansion factor $a \leq 3$ has a weak dependence on χ for the range of parameters relevant to the FMKs (e.g. Klein et al. 1994).

3.2. Flux distributions

It is instructive to estimate a power-law index of the flux distribution function $N(S)$. The index, defined as $\alpha = \log N/\log S$, is constant for a relatively narrow flux band. We discuss both thermal and nonthermal emission models described above.

(i) For FMKs of velocity above $v_0(\mathcal{R})$ the postshock electron temperature could be higher then 8 keV. Thus, the 2-8 keV photon flux S studied in the *Chandra* sample depends only weakly on the knot velocity, while $S \propto \mathcal{R}^3$. The distribution ψ is not constrained by current observations and modeling. We simply assume $\psi(v,\mathcal{R}) \propto \mathcal{R}^{-\beta} v^{-\eta}$ in a relatively narrow range of $\mathcal{R}$. Then, integrating the distribution $\mathcal{N}(v,\mathcal{R})$ over velocity (above the threshold $v_0 \propto \mathcal{R}^{-1/2}$ to reach the temperature above 8 keV) and using $S \propto \mathcal{R}^3$, we obtain the local index estimation for the thermal emission $\alpha = -4/3 + \eta/6 - \beta/3$. The index is consistent with $\alpha = -1.7 \pm 0.2$ obtained by M03 for the *Chandra* GC sample, if the initial distributions $\psi(v,\mathcal{R})$ satisfy $-3.4 < \eta - 2\beta < -1.0$.

(ii) The nonthermal flux distributions depend on the diffusion regime of the accelerated particles inside FMKs. The dependence of the diffusion coefficients on the FMK size is poorly known. Thus as an illustration we estimate the nonthermal logN–logS index α only for an ensemble of FMKs of the same size $\mathcal{R}$. We use the relation $S \propto v^\zeta$ discussed above to get $\alpha = -\eta/\zeta - 1$. Since the simulated index $\zeta \approx 0.6$, the logN–logS distribution index α would be consistent with the *Chandra* sample data for the initial velocity distributions with $\eta < 0.8$. The value of $\eta \lesssim 1$ agrees with the velocity distribution of FMKs simulated by Kifonidis et al. (2003).

4. Conclusions

Any SN event in the GC region is expected to produce many hundreds of fast moving fragments of mass $\sim 10^{-3} M_\odot$. If a SN ejects $\mathcal{N}_\star \sim 500$ FMKs of velocity 5,000 km s^{-1}, the FMKs would carry about 10% of the SN kinetic energy. Three SNRs during the last 1,000 years could produce an ensemble of more than 1,500 FMKs in the GC region providing a normalization of the logN–logS consistent with the *Chandra* data. The filamentary features apparent in the *Chandra* images of the GC region could be also relevant to the SN activity.

Fast moving SN ejecta fragments interacting with the dense GC environment provide a fast conversion of SN kinetic energy into the IR and the X-ray emission. The X-ray spectra of the fragments (with $L_{\rm x} \leq 10^{33}$ erg s^{-1} per FMK) are hard. They contain thermal and power law components with possible Fe lines. Both 6.7 and 6.4 keV lines are expected, depending on the FMK ionization structure and the relative strength of the nonthermal component. The total equivalent width is about 500 - 600 eV for a Fe mass of $\sim 10^{-4}\ M_\odot$. The hard color ratio hr is $\lesssim 0.2$ without Fe lines, while it is ~ 0.3–0.4 for a Fe mass of $\sim 10^{-4}\ M_\odot$. The medium color hr is ~ 0.4.

The spatial density of the FMKs brighter than some fixed luminosity $\mathcal{L}_0$ scales $\propto n_{\rm a}^\gamma(r)$ with the ambient gas density. This is because $L_{\rm x} \propto n_{\rm a}^\nu$ for a single FMK, while $\mathcal{N} \propto n_{\rm a}^{-1}$ from Eq.(2). The index $\gamma = -\nu(\alpha+1) - 1$ depends on the logN–logS distribution. For the thermal emission model $\nu = 2$. That implies a global decrease in the spatial density of the sources $\propto n_{\rm a}^{0.4}(r)$ (for $\alpha = -1.7$) away from Srg A*, though strong local fluctuations could appear. The apparent surface density of the FMKs would depend on the symmetry of the SN distribution (e.g. disk or spherical). The global distribution of the FMKs is expected to be an ensemble of coherent shell- and jet-like structures of a few *arcmin*-scale.

Acknowledgements. I thank the referees for helpful comments. The work was supported by RBRF 03-02-17433, 01-02-16654.

References

Aschenbach, B. 2002, In: Neutron Stars, Pulsars and Supernova Remnants. Proc 270 WE-Heraeus seminar, eds. W.Becker et al. , MPE, p.13

Baganoff, F.K., Maeda, Y., Morris, M. et al. 2003, ApJ, 591, 891

Blitz, L., Binney, J., Bally, J., Lo, K.Y. & Ho, P.T. 1993, Nat, 361, 417

Bocchino, F. & Bykov, A.M. 2003, A&A, 400, 203

Bykov, A.M. 2002, A&A, 390, 327

Chevalier, R.A. 1999, ApJ, 511, 798

Chevalier, R.A. & Kirshner, R.P. 1979, ApJ, 233, 154

Cid-Fernandes, R., Plewa, T., Rozyczka, M. et al. 1996, MNRAS, 283, 419

Fesen, R.A., Morse, J.A., Chevalier, R.A. et al. 2002, AJ, 122, 2644

Kifonidis, K., Plewa, T., Janka, H.-Th. & Müller, E. astro-ph/0302239

Klein, R.I., McKee, C.F., & Colella, P. 1994, ApJ, 420, 213

Maeda, Y., Baganoff, F.K., Feigelson, E.D., et al. 2002, ApJ, 570, 671

Mewe, R. 1990 In: Physical Processes in Hot Cosmic Plasmas, W.Brinkmann et.al. (eds.), Kluwer, p. 39.

Mezger, P.G., Duschl, W.J., & Zylka, R. 1996, AARev, 7, 289

Muno, M.P., Baganoff, F.K., Bautz, M.W., Brandt, W.N., et al. 2003, ApJ, 589, 225 (M03)

Muno, M.P., Baganoff, F.K., Bautz, M.W., Brandt, W.N., et al. 2003a, astro-ph/0308335

Rybicki, G.B. & Lightman, A.P. 1979, Radiative Processes in Astrophysics, J.Wiley & Sons, NY.
Tanaka, Y., Miyaji, T. & Hasinger, G. Astron. Nachr. 1999, 320, 181
Wang, C-Y. & Chevalier, R.A. 2002, ApJ, 574, 155
Wang, Q.D., Gotthelf, E.V. & Lang, C.C. 2002, Nat, 415, 148